Carbohydrate Polymers 345 (2024) 122537

Contents lists available at ScienceDirect

Carbohydrate Polymers

journal homepage: www.elsevier.com/locate/carbpol

Edible structuring agent shaped via interfacial precipitation on solid template: Crosslinked starch colloidosome

Peilong Li [a,1], Jieying Li [a,1], Jacob Levin [a], Arkaye Kierulf [b], James Smoot [b], Zoe Atkins [a], Leila Khazdooz [a], Amin Zarei [a], Melanie Marshall [a], Alireza Abbaspourrad [a,*]

[a] Department of Food Science, Cornell University, Ithaca, NY 14853, USA
[b] Tate & Lyle Solutions USA LLC, 5450 Prairie Stone Pkwy, Hoffman Estates, IL 60192, USA

ARTICLE INFO

Keywords:
Starch
Crosslink
Granular suspension
Rheology
Colloidosome
Pickering emulsion

ABSTRACT

Water-permeable hollow starch particles alter the rheological behavior of their granular suspensions. However, their thin shells can rupture limiting applications. In this study, we used amaranth starch as building blocks (1 μm) to craft a crosslinked superstructure. Pickering emulsions were used as the templates where starch coated the droplets. Emulsions were heated at 75 °C to induce interpenetration of the polymers followed by precipitation in ethanol to trigger colloidal fusion. Particles were then crosslinked by sodium tri-metaphosphate; hollow particles formed after the interior template was removed by hexane. When canola oil was used, the particles ruptured at pH 11.5 due to the repulsion between the strands. In contrast, palm oil, emulsified at 50 °C, formed a rigid core after cooling, locked the starch at the surface and retained the structure. The crosslinked colloidosomes were larger (89 μm) and exhibited higher viscosity, and stronger stability. Larger particles (>100 μm) were produced using higher templating volume. Gentle centrifugation to harvest the particles kept the shells intact. The hollow structure exhibited jamming transition above 10 w/w%, which could serve as a super-thickener. This work demonstrates that microarchitecture plays a critical role in shaping material functionality.

1. Introduction

Granular suspensions are mixtures of a fluid and particles, such as starch slurries, that have broad use because of their viscoelasticity. The rheological behavior of a granular system is governed by the volume fraction of particles, as the presence of large granules act as obstacles altering the flow pattern (Tanner, 2018). At low volume fractions (Φ) of non-Brownian particles the viscosity increases linearly with volume fraction (Einstein, 1905); at higher volume fractions the hydrodynamic interactions become stronger and interfere with flow trajectory, resulting in a steep increase in viscosity (Batchelor, 1977). The jamming transition of granular suspensions, where particles are in contact thus immobilizing fluid flow between particles is arrested, leads to the formation of a solid-like material (Mewis & Wagner, 2012). This dense packing phenomenon has been widely utilized in various applications, from robotic fabrication to the food industry (Assenza & Mezzenga, 2019; Mezzenga et al., 2005; Shintake et al., 2018). The viscosity of dense granular suspensions is affected by critical packing fraction (Φ_{max}):

$$\eta = \eta_0 \left(1 - \Phi/\Phi_{max}\right)^{-2} \quad (1)$$

indicating that as the volume fraction (Φ) approaches Φ_{max}, the increase in viscosity becomes more pronounced (Mewis & Wagner, 2012). This suggests that to increase the viscosity of a suspension, it would be advantageous to use particles with an easier jamming transition.

Hollow particles can significantly affect the critical packing fraction, with lower solid content required to reach the same packing fraction as dense solid particles. For example, a 40-μm hollow sphere with a one-micron-thick shell only requires 14 w/w% solids to achieve the packing as a solid sphere of the same size, resulting in a lower amount of required materials. For instance, if starch granules are crafted into a hollow structure, they can provide a bulky volume with less solid mass and potentially serve as low-carbohydrate thickeners in food applications.

Conventional starch modification enhances starch thickening ability through hydrothermal treatment, where heat dissociates the hydrogen

* Corresponding author.
E-mail address: alireza@cornell.edu (A. Abbaspourrad).
[1] These authors contributed equally to this work

https://doi.org/10.1016/j.carbpol.2024.122537
Received 17 May 2024; Received in revised form 12 July 2024; Accepted 22 July 2024
Available online 23 July 2024

bonds in the semicrystalline structure of starch, allowing the granules to soften and to swell as they absorb water (BeMiller & Huber, 2015). Modification of the morphological structure of starch is another potential direction where, in addition to swelling and water binding, this kind of modification could alter the jamming behavior of the particles which could enhance viscoelasticity. Although starch morphological modifications such as fabrication of fibers (Angel et al., 2024), nanoparticles (Dong et al., 2022), and porous starch (Zhang et al., 2024) have been explored, fabrication of hollow starch structures is new.

To fully understand the impact of hollow structures on rheological behavior, our research group recently developed a water-permeable hollow particle using starch as the starting material (Kierulf et al., 2024; Li et al., 2024). The synthetic method involved using amaranth starch as the stabilizer to prepare Pickering emulsions. Amaranth starch has the smallest naturally-occurring granular size (1 μm) (Dhital et al., 2015), and it is able to stabilize oil-in-water emulsion droplets in the tens of micrometers range (Zhu, 2019). When these emulsions were heated, the starch crystalline structure was ruptured, which allowed water to seep in; the softened starch particles at the interface then fuse together via tangled carbohydrate strands and become an integrated single layer. These hydrated starch granules were found still remaining on the emulsion interface (Sjöö et al., 2015). Ethanol was then added as an antisolvent to extract the water from the interface, triggering an interlocking of starch polymers. As a result, the interlocked starch polymers form a rigid layer of starch as a shell. When the organic template used for the core was removed, the colloidosomes with hollow interiors were obtained. Thermal activation exposed hydroxyl groups from the semicrystalline polymorph of the starch allowing water to diffuse into the core of the hollow particles via capillary action. The resulting suspension exhibited higher viscosity compared to native starch, and its microstructure can be fine-tuned during the fabrication process.

While promising, the thin shell of large hollow particles can rupture during fabrication. Without anything in the center to support them, these hollow particles are fragile under shear stress, collapsing into flat sheets rather than holding their three-dimensional, spherical form. These sheets do not have a sufficient void volume, thus weakening hydrodynamic forces, more solid is required to achieve tight packing. The vulnerability of the structure is more pronounced when the hollow particles are water-permeable. Upon hydration, the particles lose their stiffness as polymer strands from neighboring starch granules become disentangled or even dissolved under shear stress. The soft shell with lower yield stress can be ruptured by a velocity gradient induced by shear. The fragility of hollow particles presents a challenge when studying their rheological behavior and limits their uses, as the universal mechanical stress present in industrial processing, such as pumping and agitation, could break the particles, leading to inconsistency in their rheological behavior. Therefore, developing hollow particles with a strengthened shell structure is required for practical use in industries. A sturdier structure would also help to fundamentally elucidate its contribution to the rheological behavior of granular suspensions. To improve robustness, a possible approach is to crosslink the hollow particles so that the starch shell is not only physically fused to neighboring particles through tangled polymer strands, but these strands are then also covalently bound (Fig. 1A).

Crosslinked starch has been developed and polymer strands resist dissociation, however, it is still questionable if the hollow structure can survive a crosslinking reaction as the conditions usually require high pH (Hong et al., 2015; Punia Bangar et al., 2024). We hypothesize, therefore, that switching from a liquid oil core template such as canola oil to solid core template such as palm oil will allow the starch particles to retain their hollow structure under the crosslinking conditions. As a

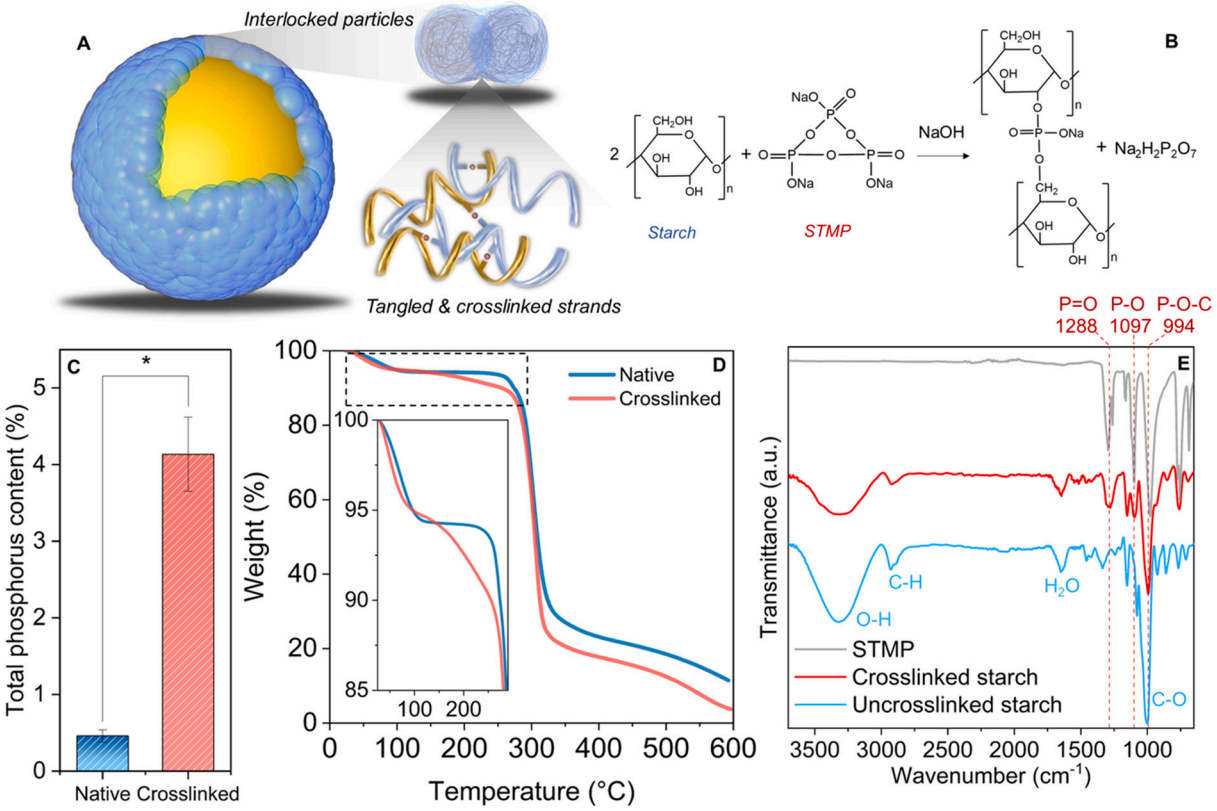

Fig. 1. (A) Schematic diagram of crosslinked starch hollow particles template on Pickering emulsion. (B) Schematic diagram of crosslink reaction using sodium trimetaphosphate (STMP). (C) Total phosphorus content (%) before and after crosslink. (D) Weight loss (%) of uncrosslinked and crosslinked starches measured by thermogravimetric analysis. (E) Fourier-transform infrared spectroscopy (FTIR) of STMP, uncrosslinked starch, and crosslinked starch.

result, the hollow particles will be more robust, and have enhanced structural stability during storage and processing with less dissociation of polymer strands. Previously uninvestigated, the successful fabrication of crosslinked hollow particles would resolve the current gap in research and indicate the rheological potential of a strengthened shell structure.

2. Materials and methods

2.1. Materials

Amaranth flour was purchased from Walmart Supermarket (Brand name: Bob's Red Mill, Inc., Milwaukie, OR, USA). Nile red, fluorescein isothiocyanate-dextran (FITC-dextran, MW = 500 kDa, catalog number: 46947), absolute ethanol, sodium tri-metaphosphate (STMP), sodium hydroxide, hexane, and polyoxyethylenesorbitan monooleate (Tween 80, MW = 1310 g/mol, catalog number: P1754) were purchased from Sigma-Aldrich (St. Louis, MO, USA). Canola oil and palm oil were purchased from Crisco (Parsippany, NJ, USA) and Okonatur (Miami, FL, USA), respectively.

2.2. Starch extraction

Amaranth starch was obtained from amaranth flour using a previously established extraction method (P. Li et al., 2022). Amaranth flour was steeped in a NaOH solution (0.15 % *w/v*). Sieving (270-mesh, VWR, PA, USA) and centrifugation (3000 *g*, Beckman Coulter, CA, USA) were used to remove crude fiber and soluble protein, respectively. The starch was collected and freeze-dried (Labconco 7740020, MO, USA), with 0.8 w/w% protein residue. The amylose content of extracted starch is 7.2 %.

2.3. Fabrication of starch hollow particles

The extracted amaranth starch was used as a Pickering stabilizer to create an oil-in-water emulsion. Canola oil or palm oil (30 w/w%) was selected as the food-grade interior template. The starch-to-oil ratio was 1:10 (w/w). The emulsification batch size was either 20 g or 60 g. To prepare the emulsions, starch powder was dispersed in water and oil was added. For palm oil, the mixture was incubated at 50 °C to melt the palm oil. The mixture was sheared with a homogenizer (T25 digital Ultra-Turrax, IKA, NC, USA) at 16,000 rpm for 1 min to create a Pickering emulsion at 50 °C and then cooled to room temperature. The resulting emulsions were then heated in a water bath (75 °C), and the emulsion temperature was monitored. When the emulsion temperature reached 70 °C, it was cooled by immersion in an ice bath for 5 min. The cooled gelatinized emulsion (60 g) was transferred dropwise into absolute ethanol (240 mL). To crosslink starch, 3 mL 10 *w/v*% STMP in water was added to the starch-in-ethanol suspension and the pH was adjusted to 11.5 using 1 M NaOH. This mixture was then incubated at room temperature for 18 h. To collect the solid from suspension, it was either centrifuged at 20 *g* for 5 min or vacuum-filtered at 30 kPa. The collected sediment was washed two more times with absolute ethanol to remove additional moisture. To remove the internal oil phase, the ethanol-purified particles were washed three times with hexane (50 °C) and centrifuged at 20 *g* for 5 min, and the solvent was evaporated in a vacuum desiccator.

2.4. Particle size analysis

The emulsion droplet size of Pickering emulsions and hollow particles was analyzed using an inverted phase contrast microscope (Nikon Eclipse TE300, NY, USA) with a digital camera (Andor Zyla sCMOs, Oxford Instruments, Abingdon, UK). Particle size was determined by analyzing >300 objects using ImageJ software (v1.51, National Institute of Health). The Sauter mean diameter was calculated as:

$$D_{3,2} = \left(\Sigma n_i d_i^3\right) / \left(\Sigma n_i d_i^2\right) \quad (2)$$

2.5. Scanning electron microscopy

The morphology of the dry starch particles was analyzed by scanning electron microscopy (SEM) (Zeiss Gemini 500, Jena, Germany) after coating the samples with gold-palladium using a sputter coater (Denton Desk V, NJ, USA) for 40 s at 30 mA and 2×10^{-4} mbar. The coated samples were visualized at 1 keV.

2.6. Confocal laser scanning microscopy (CLSM)

Nile red was used as a liposoluble fluorescent probe and mixed with palm oil at 50 °C (50 μg/mL) (Huang et al., 2021). The stained palm oil was used as the emulsion template as stated above. The aqueous phase was then stained with FITC-dextran (1 mg/mL). Starch particles at the interface swell and uptake FITC-dextran upon thermal activation which then can be used to fabricate hollow particles as stated above. The emulsion and the resultant hollow particles were examined with a confocal-laser scanning microscope (710, Carl Zeiss, Göttingen, Germany) at the excitation/emission wavelength of 514/654 nm for Nile red, 488/522 nm for FITC-dextran, with and without brightfield.

2.7. Thermogravimetric analysis (TGA)

Thermal stability of starch samples was evaluated using TGA (TA Instrument 5500, New Castle, DE, USA) with platinum sample pans under an atmosphere of nitrogen and a heating rate of 10 °C/min ramping to 600 °C.

2.8. Phosphorus analysis by inductively coupled plasma (ICP) spectroscopy

The total phosphorus content was analyzed to assess cross-linking. Starch samples (0.5 g) were subjected to digestion using concentrated nitric acid (8 mL) and hydrochloric acid (2 mL) at ambient temperature for 10 min, followed by an additional 10 min of 1 mL of 30 % hydrogen peroxide. Samples were then further digested using a CEM Microwave Accelerated Reaction System (MARS6) with MarsXpress Temperature Control and Xpress Teflon PFA vessels with Kevlar/fiberglass insulating sleeves. Microwave digestion ramped to 135 °C in 10 min and held for 3 min, which then ramped to 200 °C in 12 min and held for 15 min. Subsequently, vessels were brought to a 50-mL volume, and were analyzed using an ICP radial spectrometer (iCAP Pro XP, Thermo Fisher Scientific, NY, USA).

2.9. X-ray photoelectron spectroscopy (XPS)

Starch samples were analyzed using XPS (Scienta Omicron ESCA 2SR, Uppsala, Sweden) with operating pressure of 1×10^{-9} Torr using a pass energy of 200 eV for wide/survey scans.

2.10. Solid-state ^{31}P nuclear magnetic resonance spectroscopy (NMR)

Solid-state ^{31}P cross-polarization magic angle spinning (CP/MAS) NMR measurements were recorded by a DSX-500 Bruker (11.7 T, MA, USA) operating at 202.5 MHz for the ^{31}P nucleus. A 4 mm Bruker MAS NMR probe was used for the measurement, and H_3PO_4 was used as the chemical shift reference. For all measurements, spinal ^{1}H-decoupling was applied during signal acquisition using two-pulse phase modulation (TPPM). ^{31}P CP/MAS NMR spectra were acquired with a 12 KHz spinning rate, 4 ms contact time, and 12 s recycle delay.

2.11. ^{13}C NMR and solid-state ^{13}C NMR

Solution state ^{13}C NMR at 125 MHz was performed using a Bruker Avance-500 spectrometer (Bruker, MA, USA) chemical shifts were

recorded in δ (ppm) and referenced to tetramethylsilane. Solid-state ^{13}C NMR spectra were obtained using CP/MAS on a DSX-500 Bruker spectrometer (11.7 T, MA, USA) operating at 125.8 MHz. A 4 mm Bruker MAS NMR probe facilitated the measurements. Spinal ^{1}H-decoupling was applied during signal acquisition using two-pulse phase modulation (TPPM). The sample was spun at a rate of 10 kHz, with a cross-polarization contact time of 0.5 ms and a recycle delay of 2 s.

2.12. Preparation of simulated salad dressings

A 50 w/w% olive oil-in-water emulsion was used as a simulated salad dressing. To 22.5 mL of water, 2.5 g of Tween 80 was added. Olive oil (25 g) was then added, and the mixture was emulsified using a high-shear homogenizer (T25 digital Ultra-Turrax, IKA, NC, USA) at 10,000 rpm for 2 min. A reduced fat emulsion with 20 w/w% oil was prepared by diluting the 50 w/w% emulsion with water proportionally. Starch hollow particles (1 or 5 w/w%) were added to replace fat in the simulated salad dressing.

2.13. Rheological measurements

To measure viscosity, a rheometer (Anton Paar MCR501, Graz, Austria) was used with a 25 mm parallel plate set to a 0.5 mm gap. Starch suspensions were tested at a temperature of 20 °C. A 15 w/w% suspension was used if not specified. The shear stress (τ) and shear rate ($\dot{\gamma}$) were used to fit a Herschel-Bulkley model:

$$\tau = \tau_0 + \kappa\dot{\gamma}^n \quad (3)$$

where κ is the consistency factor, τ_0 is the yield stress, n is the flow index. To test the stability of the samples against mechanical stress, a secondary shear ramp was conducted after 30 s of resting and the viscosity retention was evaluated. Storage stability of hydrated hollow particles was tested by measuring viscosity retention after the suspension was stored at room temperature for one week. Thermal stability was tested by measuring viscosity retention after heating at 90 °C for 30 min. Acid stability was tested by measuring viscosity at pH 3.

2.14. Statistical analysis

Statistical analysis was performed using one-way analysis of variance (ANOVA) and Tukey's multiple comparison test in JMP Pro (Version 17, SAS Institute, USA) with a significance level set at $p < 0.05$ to determine any significant differences. For non-normal distributions, the nonparametric Wilcoxon method was used for comparison.

3. Results and discussion

3.1. Manipulation of interior template to fabricate crosslinked colloidosome

To enhance the robustness of the hollow structure we crosslinked the starch cages to chemically stitch the polymer strands together. Therefore, the starch particles at the interface are expected to behave as a single object improving mechanical and storage stability (Fig. 1A). The crosslink reaction begins with ring opening of sodium tri-metaphosphate (STMP) followed by phosphorylation of the hydroxyl groups on the carbohydrate chains. The resulting starch triphosphate then reacts with another starch molecule via the α-phosphate bond, producing distarch phosphate and pyrophosphate at basic pH levels (Fig. 1B) (Narayanan et al., 2015). The total phosphorus content of native starch was <0.5 w/w% (Fig. 1C), which can be attributed to the minor residual phospholipids in the amylose helices. After crosslinking, the total phosphorus content increased significantly to 4 w/w% due to phosphorylation (Fig. 1C).

TGA shows an initial sharp drop in mass under 100 °C which can be attributed to ~6 w/w% moisture present in native starch. After 100 °C the samples maintain their weight until the temperature increases to 254 °C at which point they decompose (Fig. 1D). The crosslinked starch exhibited weaker thermal stability where a continuous weight loss was observed from 100 to 250 °C. This was not unexpected however, because at temperatures above 150 °C, orthophosphates are known to convert to pyrophosphates and lose weight through a condensation mechanism (Banach et al., 2009; Liu et al., 2016).

Phosphorylation was confirmed by the FTIR spectra that showed a P═O in phosphate ester at 1288 cm^{-1} (Fig. 1E), which is absent from samples of the non-crosslinked starch. A new band was also observed at 1097 cm^{-1} after the reaction, owing to the P—O stretching vibration. The band P-O-P shown at 980 cm^{-1} of STMP shifted to the left (994 cm^{-1}) after the reaction, signifying the formation of a P-O-C bond (Fig. 1E) (Silverstein et al., 2014).

X-ray photoelectron spectroscopy (XPS) provided more information about the chemical composition of crosslinked starch (Fig. 2A-D). Carbon and oxygen were the major elements. The peaks of C 1 s were deconvoluted. Aside from the typical bonds in the starch carbohydrate backbone, C—N and C═O were also observed, which can be attributed to the residual protein content. The protein remaining on the starch contributed to its emulsifying and templating ability (P. Li et al., 2024). The characteristic peak of P 2p was deconvoluted to P═O, P—O, and P-O-C (Wu et al., 2022). The ^{31}P CP/MAS NMR spectrum shows that the majority of phosphorus was from phosphorylated starch and only a small amount was from free STMP residuals (Fig. 2E). The deconvoluted peaks showed that distarch monophosphate (DSMP) was the most abundant product (69.4 %) at −0.4 ppm indicating that the fused polymer strands can be chemically stitched. Side products were also found, including monostarch monophosphate (MSMP, 20.3 %) and monostarch diphosphate (MSDP, 10.3 %) (Kierulf et al., 2024).

When using canola oil as the organic phase, the Pickering emulsion showed multimodal distribution of droplet size (Fig. S2) with a Sauter mean over 100 μm (Fig. 3A). The emulsion was further thermally processed so the starch molecules dissociated from their original helical semicrystalline state and the granules swelled with water (Fig. 3B). Polymeric starch strands possess higher conformational freedom, allowing them to entangle, causing the closely packed neighboring granules to interpenetrate and form a cohesive structure (Li et al., 2022). Because ethanol acts as an antisolvent to starch (Dong et al., 2022), when the gelatinized emulsion is introduced to absolute ethanol, the starch particles anchored at the interface lose water-holding capacity. Consequently, the water is removed from the starch layer, the interface shrinks, and the interlocking particles on the interface form a shell. During antisolvent precipitation, we observed that many oil droplets were squeezed out as the starch interface shrinks where the bright oil droplets were uncovered (Fig. 3C). This is due to the moisture extraction during antisolvent precipitation which causes sudden shrinkage of the shell building up internal stress and leading to the inability to hold the interior. The shell was subsequently washed with hexane to eliminate any residual template, such as canola oil in the core or ethanol in the continuous phase (Fig. 2E). The hollow particles formed were smaller (68.6 μm, Fig. 3J) compared to the original emulsion template (Fig. 3A). We attribute this to the fragility of the larger particles which break during antisolvent precipitation leaving behind only the smaller colloidosomes (Fig. 3G).

To improve structural robustness, the precipitated particles were crosslinked using STMP. However, after crosslinking, more free particles were observed in the samples templated with canola oil. The free starch particles had been removed from the oil droplets, resulting in an uncovered surface (Fig. 3D). After the oil was removed, the interface collapsed (Fig. 3F) and the starch formed dense clumps (Fig. 3H). The collapse of the colloidosomes after crosslinking can be attributed to the elevated pH (11.5) required for the formation of distarch monophosphate (Hong et al., 2015). Alkaline conditions were reported to dissociate the hydrogen bonds between the strands and create a negative

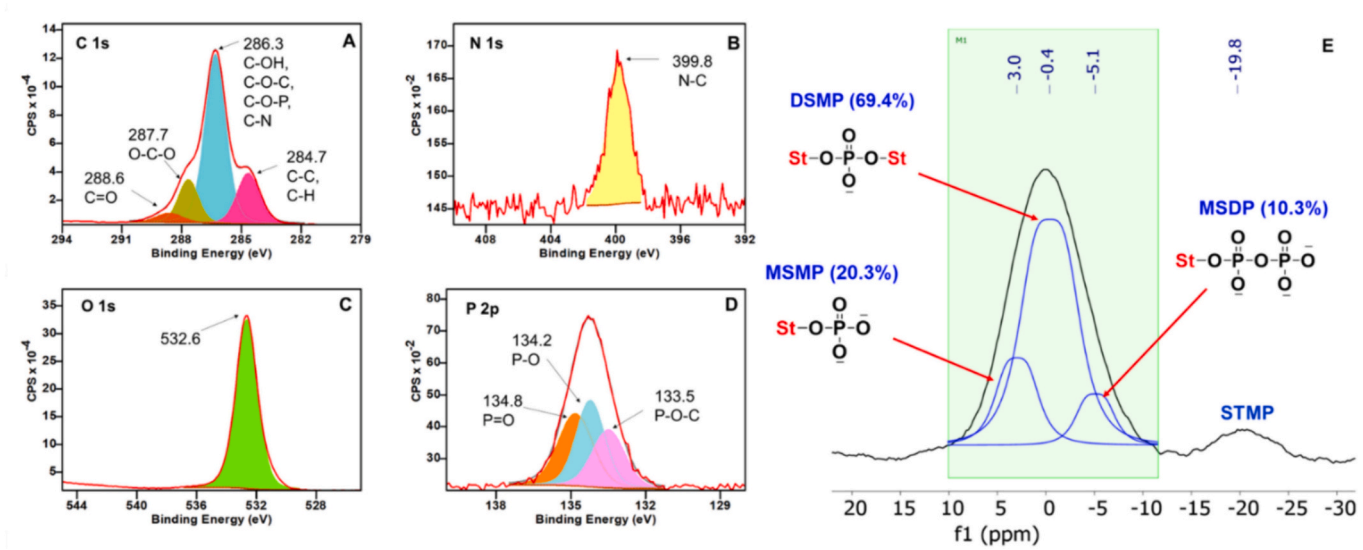

Fig. 2. C 1 s XPS spectra (A), N 1 s XPS spectra (B), O 1 s XPS spectra (C), P 2p XPS spectra (D), and CPMAS solid-state ^{31}P NMR spectra of crosslinked starch (E). Peakes are deconvoluted for phosphorylated products: monostarch monophosphate (MSMP), distarch monophosphate (DSMP), and monostarch diphosphate (MSDP).

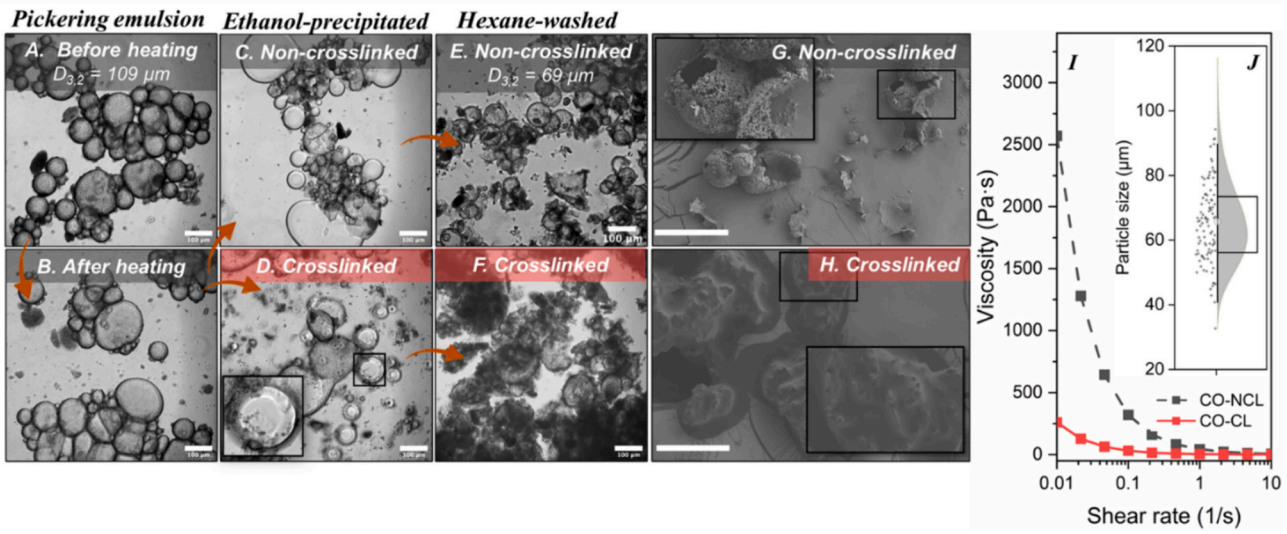

Fig. 3. (A-H) Microstructure at different stages of fabrication process of non-crosslinked and crosslinked hollow starch using canola oil as the template. The bright oil droplets observed in Fig. 3C and D indicate that the oil phase was squeezed out from the starch shell. The scale bars are 100 μm. (I) Viscosity of non-crosslinked (NCL) and crosslinked (CL) hollow starch suspensions using canola oil (CO) as the template. (J) Particle size distribution of non-crosslinked hollow particles. The box chart represents 25th and 75th percentiles with median indicated as the middle.

charge on starch, causing the polymers to untangle due to stronger electrostatic repulsions (Majzoobi & Farahnaky, 2021). The rheological study showed that when canola oil was used as a template, the resultant starch particles showed reduced viscosity after crosslinking (Fig. 3I). This decrease in viscosity is due to the structural damage to the hollow particles and thus, the volume fraction was lower compared to the non-crosslinked particles.

Canola oil remains in the liquid state throughout the templating process, which is insufficient to retain starch on the surface. Therefore, we postulated that using a templating material that was solid at room temperature could form a more robust core from which to anchor the polymer strands, thus reducing damage during antisolvent precipitation. Therefore, we switched the organic phase to palm oil. At 50 °C, palm oil melts and the liquid state facilitates emulsification; then, when cooled to room temperature, oil droplets solidify and form a Pickering emulsion with solid internal phase. The emulsion droplets of palm oil are 85 μm, smaller than that of the canola oil emulsions, and the size distribution was more uniform (Figs. 4A and Fig. S2). The palm-oil emulsion was heated to 70 °C to melt the core and to fuse the starch interface (Fig. 4B) and then the samples were cooled again to rigidify the template. After mixing with ethanol, no squeezed-out oil was observed owing to the solid state of the template phase, suggesting that solid palm oil beads protect shell integrity at the stage of antisolvent precipitation (Fig. 4C). The solid core secured the starch at the oil droplet interface and prevented dissociation in the precipitated shell treated with STMP at pH 11.5 (Fig. 4D). The resulting crosslinked colloidosomes showed 89 μm in average size which was found to be larger compared to that of the non-crosslinked hollow particles (Fig. 4E-I). This could be due to that crosslinking helped to preserve the large hollow particles (Fig. 4G). A nonparametric Wilcoxon test showed that the particle size distribution after crosslinking was significantly wider ($p < 0.05$) than non-crosslinked, with a greater portion of large colloidosomes retained.

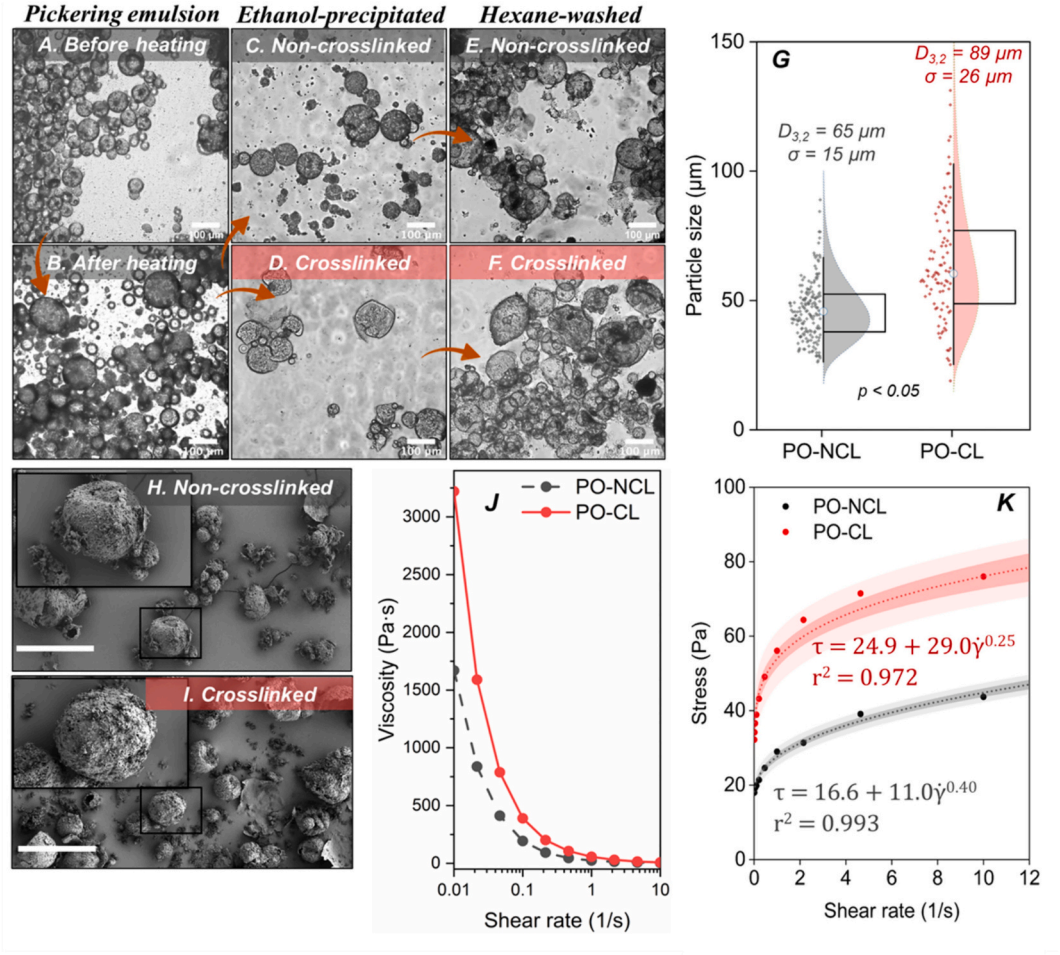

Fig. 4. (A-F) Optical microscopic photos at different stages of fabrication process (Pickering emulsion before and after heating, ethanol-precipitated particles, and hexane-washed hollow particles) of non-crosslinked (NCL) and crosslinked (CL) hollow starch using palm oil (PO) as the template. (G) Size distribution of non-crosslinked and crosslinked hollow particles. Box plots represent 25th and 75th percentiles with median indicated in the middle. Sauter mean ($D_{3,2}$) and standard deviation (σ) of each population are noted. Distribution was tested using a nonparametric Wilcoxon method ($p < 0.05$). (H—I) SEM of non-crosslinked and crosslinked hollow particles using palm oil as template. Scale bars are 100 μm. (J) Viscosity of aqueous suspension of non-crosslinked (NCL) and crosslinked (CL) hollow particles templated on palm oil. (K) Shear stress fitted to Herschel–Bulkley model. The inner and outer bands of the regression curves represent 95 % confidence intervals and 95 % prediction intervals, respectively.

The rheological study demonstrated that the crosslinked colloidosomes yielded higher viscosity compared to the corresponding non-crosslinked samples (Fig. 4J). The fitted Hershel-Bulkley model for non-Bingham plastic behavior shows that the crosslinked particles exhibited a yield stress of 24.9 Pa, higher than non-crosslinked starch at 16.6 Pa (Fig. 4K). This is likely due to the intact hollow particles with larger void space providing higher specific volume, and with narrowed space between granules the suspension provided higher hydrodynamic interactions.

The palm oil was stained with Nile red to demonstrate template formation (Fig. 5A). Fat crystals can be observed in the core of the palm oil droplets, indicating solidification. The individual starch granules, the building blocks, surround the stained palm oil particle. FTIC-dextran was then added to emulsion to stain the aqueous phase (Fig. 5B). Thermal treatment resulted in the swelling of the starch particles and subsequent uptake of water and FITC-dextran in the continuous phase of the emulsion (Fig. 5C). Upon antisolvent addition, the interfacial particles penetrate each other and interlock. The lack of Nile red fluorescence following the hexane wash indicated the removal of the internal palm oil core. Only FITC-stained shell remained (Fig. 5D).

Solid-state ^{13}C NMR spectroscopy confirmed the removal of palm oil from the particles as well as the absence of hexane in the final products (Fig. 5E-G). Solution state ^{13}C NMR of the palm oil in $CDCl_3$ was used to gauge the approximate regions where peaks would appear in the solid state NMR if palm oil persisted after washing, specifically the quaternary carbons of the carbonyl groups and the aliphatic protons of the saturated side chain (Awogbemi et al., 2022) (Fig. 5E). The unwashed particles also exhibited weak peaks at 72.6 and 62.1 ppm, which are attributed to starch. Because the starch shell is much thinner compared to the palm oil interior (starch:oil = 1:10, w/w), therefore, the signal intensity of the starch was lower compared to the peaks of palm oil (Fig. 5E-G). After three cycles of purification using hexane at 50 °C, the intensity of palm oil decreased substantially (Fig. 5G). The solid-state ^{13}C NMR spectrum of the hexane-washed particles confirmed that nearly all the palm oil had been removed. The trace amount of remaining palm oil does not pose a toxicity concern, as it is a common food ingredient; the hexane was evaporated as well, thus the hollow starch can safely be used in food applications (P. Li et al., 2024).

A suspension of hollow particles was evaluated for its stability to mechanical stress (Fig. 6). Comparing the viscosity before and after shear (Fig. 6A), non-crosslinked starch showed weak viscosity retention (40 % of the viscosity before shear). Microscopic examination with image processing demonstrated that after shear, there was an extensive dissociation (33 % particle-size reduction) of starch particles in the non-crosslinked samples (Fig. 6B and C). In contrast, the crosslinked samples were more robust and more intact large particles remained (Fig. 6E and

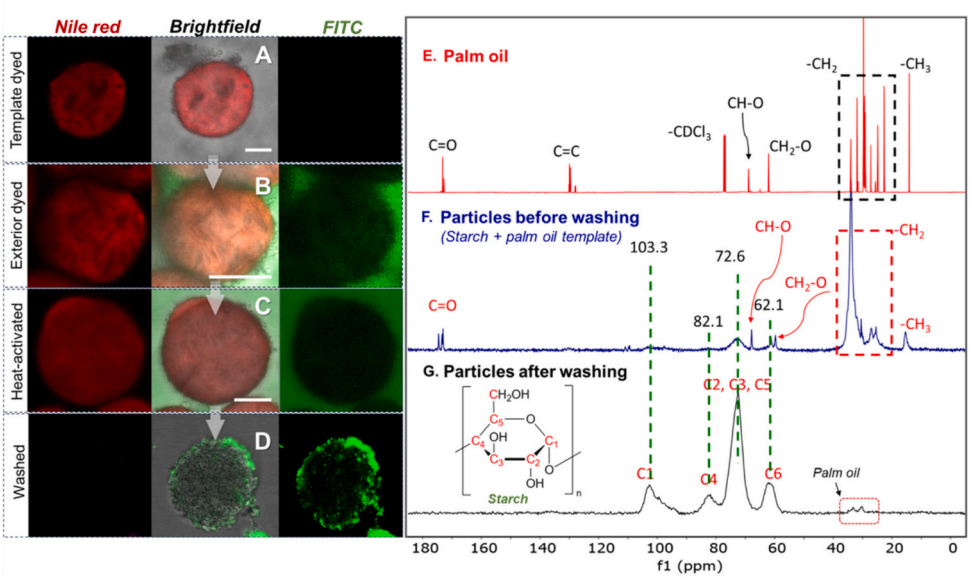

Fig. 5. CLSM photos of template-stained emulsion (A), exterior-stained emulsion (B), particles with thermal-fused interface (C), and hexane-washed hollow particles (D). Photos were captured in different emission channels for Nile red and FITC, and overlaid on a brightfield image. Scale bars are 20 μm. (*E*-G) Comparison of ^{13}C NMR of palm oil in $CDCl_3$ with solid-state ^{13}C NMR of particles before and after washing with hexane.

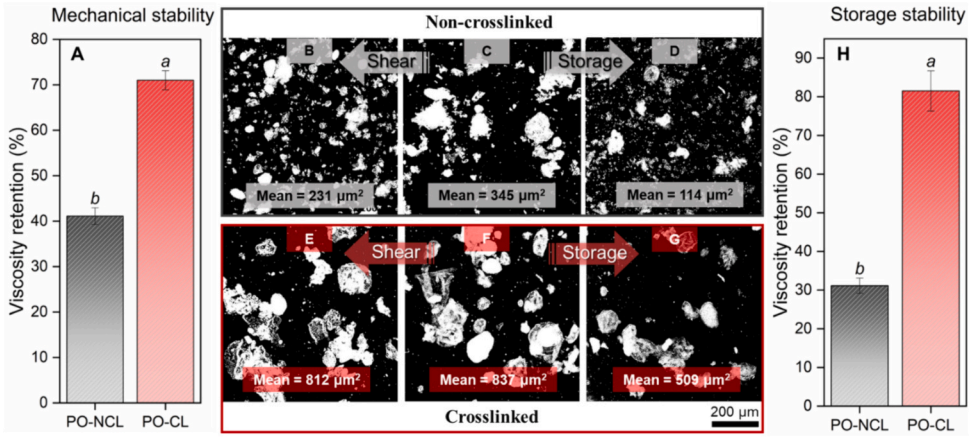

Fig. 6. Mechanical stability and storage stability of crosslinked (CL) and non-crosslinked (NCL) hollow starch using palm oil (PO) as the template. (A) Viscosity retention (%) of starch suspension after shearing. (B—D) Image processing of non-crosslinked hollow particles after shear, before shear, and after soaking for 7 days, respectively. Size of dissociation is evaluated by pixel analysis and noted as area (μm^2) (E-G) Image processing of crosslinked hollow particles after shear, before shear, and after soaked for 7 days, respectively. (H) Viscosity retention (%) of starch suspensions after soaking for 7 days. Scale bars are 200 μm. Letters above error bars indicate statistical differences ($p < 0.05$).

F). The enhanced structural stability enabled the suspension of crosslinked particles to retain viscosity (Fig. 6A). Overall, the data suggests that the crosslinks improved the mechanical stability of the solid template colloidosomes.

In addition to shear stability, soaking stability was studied to evaluate robustness during storage. The particles were hydrated, and the microstructure was examined after seven days. When the starch was not crosslinked, the superstructure was significantly damaged, with 67 % reduction in particle size as analyzed by imaging processing (Fig. 6D). The untangling of starch chains, for an increase in entropy, when hydrated promotes leaching and dissolving of polymers, creating an open shell structure (Koganti et al., 2011). In contrast, when the cages are crosslinked, they remain intact even after a week of soaking, because the polymer chains are covalently stitched (Fig. 6G) (He et al., 2023). The improved stability in soaking conditions suggests superior performance potential of these starch colloidosomes in food-based applications, especially those that have long shelf-lives such as canned soups or dipping sauces. While the shell crosslinking has been reported for non-food materials such as alkyne-azides (Samanta et al., 2009), polyamines (Walsh et al., 2010), organosilica (S. Li et al., 2015), this is the first time it has been shown to fabricate colloidosomes using starch as a food-safe material crosslinked by a reagent approved by the United States Food and Drug Administration (Food and Drug Administration, 1993).

Environmental conditions such as pH and temperature are important, particularly in the food industry. To evaluate the application potential, stability against cooking and acidity was also tested. When the colloidosomes were not crosslinked, the viscosity decreased significantly after heating at 90 °C for 30 min (Fig. S3A). Microscopic examination revealed that many particles dissociated after cooking (Fig. S3B, S3C), likely due to amylose leaching during heating, which disintegrated the starch shell. In contrast, the structure of the crosslinked hollow particles remained intact after thermal treatment (Fig. S3D, S3E). This is because, instead of relying on just physical entanglement, the starch molecules

are chemically bonded and can resist dissociation. The viscosity retention for cross-linked starch was >70 %, indicating that the crosslinked hollow particles can be used in products that require thermal processing, such as soups.

Acidity stability was also tested at pH 3, the lowest food-related pH. The results showed that the viscosity at pH 3 was not significantly different compared to neutral pH, regardless of crosslinking (Fig. S4). This indicates that the particles can be used in acidic foods such as salad dressings.

3.2. Roles of template crafting and harvest

Processing steps can impact the structure and functionality of a material, such as the batch volumes used for emulsification. We prepared emulsions with two different sample sizes: 20 g per batch (corresponding to a lower processing volume, shown in Fig. 7B) and 60 g per batch (corresponding to a higher processing volume, shown in Fig. 7C). The results indicated that a higher emulsification volume resulted in the formation of larger droplets due to a reduced emulsification efficiency (Fig. S1). After gelatinization, interfacial precipitation, crosslinking, and template removal, the hollow particles were produced. The emulsions fabricated at higher processing volumes produced hollow starch particles that were above 100 μm in Sauter mean diameter (Fig. 7E), while those produced at a lower batch size were smaller (Fig. 7D). A nonparametric Wilcoxon test shows that the particle size distribution produced from higher processing volume was significantly different ($p < 0.05$) than the one produced from lower processing volume, with a greater portion of large colloidosome retained (Fig. 7F).

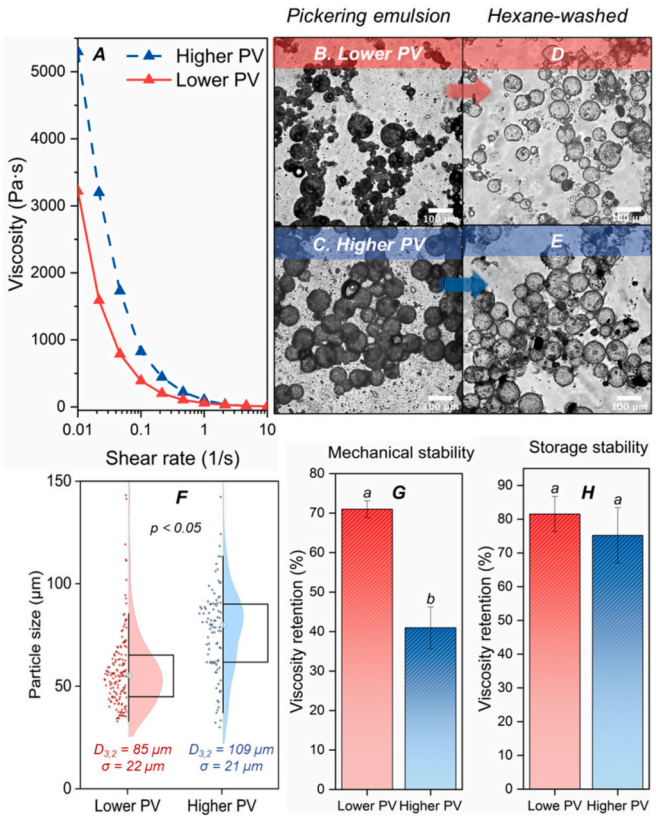

Fig. 7. (A) Viscosity of hollow starch suspensions fabricated from higher processing volume (PV) and lower processing volume. (B—C) Pickering emulsion prepared in lower (20 g) and higher processing volume (60 g), respectively. (D-E) Hollow particles prepared in lower and higher processing volume, respectively. Scale bars are 100 μm. (F) Size distribution of non-crosslinked and crosslinked hollow particles. Box plots represent 25th and 75th percentiles with median indicated in the middle. Sauter mean ($D_{3,2}$) and standard deviation (σ) of each population are noted. Distribution was tested using a nonparametric Wilcoxon method ($p < 0.05$). (G-H) Mechanical stability and storage stability of hollow starch fabricated from higher processing volume and lower processing volume. Letters above error bars indicate statistical differences ($p < 0.05$).

The rheological study shows that viscosity increased with a higher processing volume of hollow particles (Fig. 7A) because the larger hollow particles provided a higher volume fraction given the same solid content. However, the stability study suggested that the larger hollow starch particles showed lower viscosity retention (Fig. 7F), thus indicating a weaker mechanical stability, which could be due to the large objects being more fragile against shear stress due to a lower debonding fracture energy (Lauke, 2008). However, the soaking stability was not significantly affected by processing volume and both groups provided viscosity retention higher than 70 %, owing to covalent crosslink (Fig. 7H).

Besides emulsification volume, another processing factor that may alter structure is sample collection when the crosslinked samples are separated from bulk liquid. Centrifugation and vacuum filtration were both evaluated. Filtration provided high processing throughput and screens free particles (~1 μm) through filter papers with 8 μm pore size, which would be expected to increase specific volume and porosity of hollow particles. However, the results indicated that the hollow structure was damaged by vacuum filtration because the negative pressure (30 kPa) during vacuum filtration causes the oil phase to be extracted (Fig. S5C). Upon template removal, the hollow starch shrank in size and the structure collapsed (Fig. S5E), which in turn lowered viscosity (Fig. S5A). In contrast, centrifugation retained the structure (Figs. S5B and S5D). According to Stokes Law, the sedimentation velocity of suspension quadratically increases with particle size (Li et al., 2020); owing to the large particle size, a low relative centrifugal force (RCF = 20 *g*) was sufficient to separate the intact granules from bulk liquid within 5 min, without crushing.

3.3. Application of hollow starch as a food-grade thickener

The palm-oil-templated, crosslinked hollow starch was used to evaluate its potential as a thickener. The viscosity of crosslinked hollow starch and non-hollow control with the same degree of gelatinization were evaluated at different starch content (Fig. 8). The results showed that 5 w/w% non-hollow starch showed ~10 Pa·s viscosity at the shear rate of 0.01 s^{-1}, which increased with higher starch content, to $<10^4$ Pa·s with 25 w/w% solid content (Fig. 8A). Starch suspensions made with hollow starch showed significantly higher viscosity with a lower amount of starch (Fig. 8B). Suspensions of 15 w/w% hollow starch reached similar viscosity compared to suspensions with 25 % non-hollow starch. When the viscosity at 0.01 s^{-1} shear rate was plotted against starch content, a sharp increase was observed around 10 w/w% of hollow starch (Fig. 8C). This contrast can be explained by the jamming effect: the hollow starch is packed tightly given the large volume fraction, whereas the native starch granules were dispersed without significant contact (Fig. 8D-E). At lower volume fraction, particles are further apart and their flow behavior in the trajectory was not influenced by their neighbors. The force (*F*) required to squeeze the liquid at certain velocity (*v*) through the gap between two particles (radius = *r*) increases with the closer distance (*h*):

$$F = 1.5\pi\eta_0 r^2 v/h \quad (4)$$

such that the drag force is infinitely high when the particles are in contact (Mewis & Wagner, 2012). As the particles become more crowded, the interparticle friction inhibits their movement and slows down solvent flow through the narrow channels, resulting in a stronger hydrodynamic effect. In summary, hollow starch has shown superior thickening ability over its non-hollow counterpart. Thus, this label-friendly thickener can reduce carbohydrate content in food products while maintaining desired texture, making it a clean-label alternative for

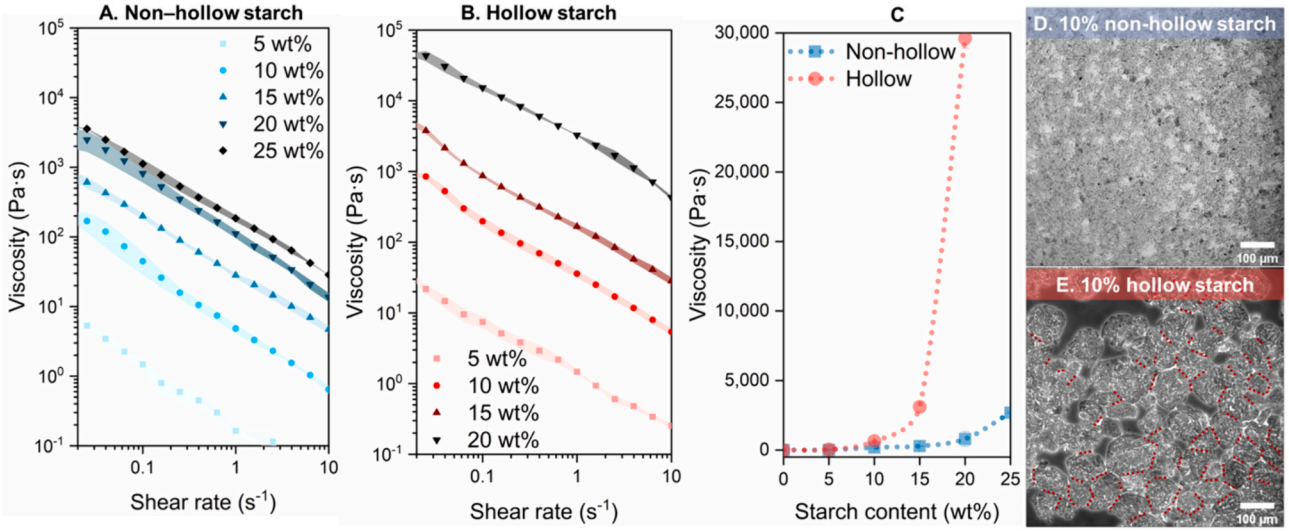

Fig. 8. (A) Viscosity of non-hollow starch suspensions with different solid content (5–25 w/w%). (B) Viscosity of hollow starch with different solid content. The shadow of curves represents the error bands. (C) Viscosity of hollow and non-hollow starch at 0.01 s^{-1} in different solid content. (D) Structure of 10 w/w% suspension of non-hollow starch. (E) Structure of 10 w/w% suspension of hollow starch. Dash lines indicate the contact between granules. Scale bars are 100 μm.

consumers seeking lower-calorie options. This is particularly favorable for the food industry as there is a growing trend towards healthier food options.

Hollow starch particles were studied within complex food matrices, such as salad dressings. We prepared a simulated salad dressing containing 50 w/w% oil content with a high calorie count (350 kcal per 100 g) and found that the oil droplets were closely packed together to create a cohesive texture (Fig. 9A). To make a reduced-fat salad dressing, 20 w/w% oil was used, decreasing droplet density (Fig. 9B) and the viscosity decreased significantly as a result(Fig. 9E). However, when 1 w/w% hollow starch was added to the 20 w/w% oil dressing, the starch occupied a significant volume, resulting in increased viscosity (Fig. 9C). When 5 w/w% hollow starch was added, the viscosity increased further as the hollow granules were packed tightly and squeezed oil droplets in between them, locally behaving similarly to the 50 w/w% oil dressing (Fig. 9D). The viscosity at a 10 s^{-1} shear rate was over 100 cP (Fig. 9E) with only 160 kcal per 100 g, half the energy of the full-fat dressing. This study indicates that hollow starch can be used as a fat replacer by taking up the volume of the oil phase and providing a cohesive texture.

4. Conclusions

In this study, we synthesized hollow particles using amaranth starch (1 μm) as edible building blocks through a bottom-up assembly on oil templates, and proved our hypothesis that the material functionality can be tuned by strengthening their microstructure. The crosslinking reaction with sodium tri-metaphosphate (STMP) at elevated pH damaged the colloidosome architecture when canola oil was used as the liquid templating phase, but switching the template to solid palm oil preserved the structure during crosslinking as the solid core retained starch particles on the interface. The crosslinked colloidosomes exhibited higher viscosity and stronger structural stability against mechanical stress, hydrated storage, and thermal processing. Fabrication procedures also affected particle functionality: higher processing volumes of emulsification produced larger templates, resulting in larger hollow particles with higher viscosity but lower stability against mechanical stress. To

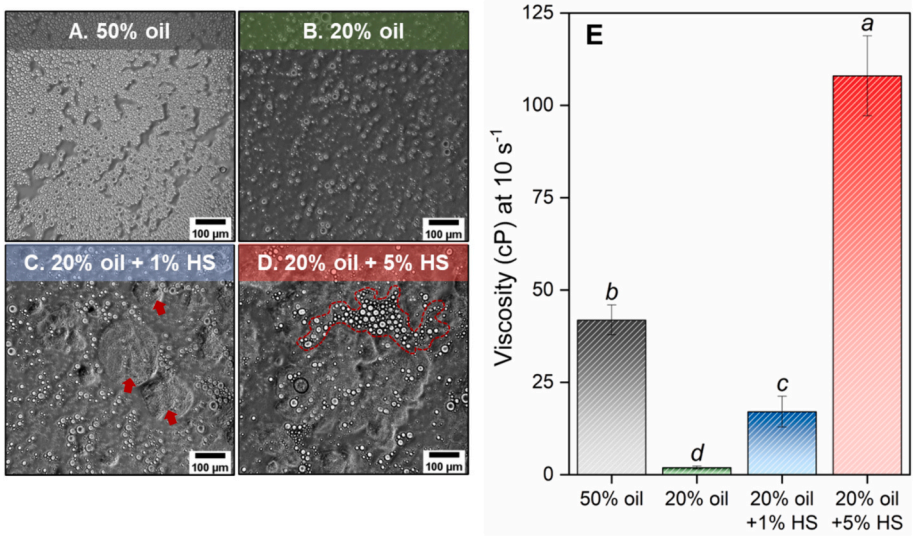

Fig. 9. Structure of emulsion-modeled dressings with 50 w/w% oil (A), 20 w/w% oil (B), 20 w/w% oil +1 w/w% hollow starch (HS) (C), 20 w/w% oil +5 w/w% hollow starch (D), and the viscosity comparison at 10 s^{-1}(E). Scale bars are 100 μm. The letters above error bars indicate statistical differences ($p < 0.05$).

collect particles, centrifugation retained the hollow structure, while vacuum filtration smashed the particles. The synthesized starch colloidosomes jammed at 10 w/w% solid content and exhibited viscosity only achievable by non-hollow starch at higher starch contents, indicating the potential of such a design as a low-carb thickening agent in future foods such as soups. Hollow starch was also evaluated as a fat substitute in low-calorie salad dressing, showing its potential as a volume-based structuring agent. This study used sustainable carbohydrate polymers to demonstrate that a robust microarchitecture modulated rheological behavior. The concept can be applied to design the new generation of texturizing materials. Future research should explore the use of commercially available starch, such as corn starch, to fabricate hollow particles for higher scalability.

CRediT authorship contribution statement

Peilong Li: Writing – review & editing, Writing – original draft, Project administration, Methodology, Investigation, Formal analysis, Conceptualization. **Jieying Li:** Writing – review & editing, Writing – original draft, Project administration, Methodology, Investigation, Formal analysis. **Jacob Levin:** Writing – review & editing, Investigation, Formal analysis. **Arkaye Kierulf:** Writing – review & editing, Project administration, Methodology. **James Smoot:** Writing – review & editing, Project administration, Funding acquisition. **Zoe Atkins:** Writing – review & editing, Formal analysis. **Leila Khazdooz:** Writing – review & editing, Formal analysis. **Amin Zarei:** Writing – review & editing, Formal analysis. **Melanie Marshall:** Writing – review & editing, Formal analysis. **Alireza Abbaspourrad:** Writing – review & editing, Supervision, Project administration, Funding acquisition, Conceptualization.

Declaration of competing interest

The authors declare that they have no known competing financial interests or personal relationships that could have appeared to influence the work reported in this paper.

Data availability

Data will be made available on request.

Acknowledgments

This project was funded by Tate & Lyle Solutions USA LLC. We would like to thank Weichang Liu from Tate & Lyle Solutions USA LLC for many fruitful and thoughtful discussions and SVP Veronica Cueva also from Tate & Lyle Solutions USA LLC for supporting the funding of this work and Sara Vinarov for legal guidance. We also thank Kelley J. Donaghy for editing this manuscript. The SEM imaging data was acquired through the NSF MRSEC program (DMR-1719875) at the Cornell Center for Materials Research Shared Facilities. The CLSM imaging data was acquired through the Cornell University Biotechnology Resource Center (RRID:SCR_021741), with NIH S10RR025502 funding. The rheological measurement was conducted at Cornell Energy Systems Institute.

Appendix A. Supplementary data

Supplementary data to this article can be found online at https://doi.org/10.1016/j.carbpol.2024.122537.

References

Angel, N., Li, S., & Kong, L. (2024). Emerging applications of nanofibers electrospun from carbohydrate polymers. *Journal of Future Foods, 4*(4), 289–299. https://doi.org/10.1016/j.jfutfo.2023.11.001

Assenza, S., & Mezzenga, R. (2019). Soft condensed matter physics of foods and macronutrients. *Nature Reviews Physics, 1*(9), Article 9. https://doi.org/10.1038/s42254-019-0077-8

Awogbemi, O., Kallon, D. V. V., Aigbodion, V. S., & Mzozoyana, V. (2022). Property determination, FA composition and NMR characterization of palm oil, used palm oil and their methyl esters. *Processes, 10(1), Article 1*. https://doi.org/10.3390/pr10010011

Banach, M., Kowalski, Z., Wzorek, Z., & Gorazda, K. (2009). A chemical method of the production of "heavy" sodium tripolyphosphate with the high content of form I or form II. *PJCT, 11*(2), 13–20. https://doi.org/10.2478/v10026-009-0018-x

Batchelor, G. K. (1977). The effect of Brownian motion on the bulk stress in a suspension of spherical particles. *Journal of Fluid Mechanics, 83*(1), 97–117. https://doi.org/10.1017/S0022112077001062

BeMiller, J. N., & Huber, K. C. (2015). Physical modification of food starch functionalities. *Annual Review of Food Science and Technology, 6*(1), 19–69. https://doi.org/10.1146/annurev-food-022814-015552

Dhital, S., Butardo, V. M., Jobling, S. A., & Gidley, M. J. (2015). Rice starch granule amylolysis – Differentiating effects of particle size, morphology, thermal properties and crystalline polymorph. *Carbohydrate Polymers, 115*, 305–316. https://doi.org/10.1016/j.carbpol.2014.08.091

Dong, H., Zhang, Q., Gao, J., Chen, L., & Vasanthan, T. (2022). Preparation and characterization of nanoparticles from field pea starch by batch versus continuous nanoprecipitation techniques. *Food Hydrocolloids, 122*, Article 107098. https://doi.org/10.1016/j.foodhyd.2021.107098

Einstein, A. (1905). On the motion of small particles suspended in liquids at rest required by the molecular-kinetic theory of heat. *Annalen der Physik, 17*(549–560), 208.

Food and Drug Administration. (1993). Food additives permitted for direct addition to food for human consumption. https://www.accessdata.fda.gov/scripts/cdrh/cfdocs/cfcfr/CFRSearch.cfm?fr=172.892.

He, X., Zhao, S., Zhang, Z., Dai, L., Qin, Y., Ji, N., Xiong, L., Shi, R., & Sun, Q. (2023). A combined extrusion, retrogradation, and cross-linking strategy for preparing starch-based straws with desirable mechanical properties. *International Journal of Biological Macromolecules, 227*, 1089–1097. https://doi.org/10.1016/j.ijbiomac.2022.11.289

Hong, J. S., Gomand, S. V., & Delcour, J. A. (2015). Preparation of cross-linked maize (Zea mays L.) starch in different reaction media. *Carbohydrate Polymers, 124*, 302–310. https://doi.org/10.1016/j.carbpol.2015.02.022

Huang, M., Wang, J., & Tan, C. (2021). Tunable high internal phase emulsions stabilized by cross-linking/ electrostatic deposition of polysaccharides for delivery of hydrophobic bioactives. *Food Hydrocolloids, 118*, Article 106742. https://doi.org/10.1016/j.foodhyd.2021.106742

Kierulf, A., Mosleh, I., Li, J., Li, P., Zarei, A., Khazdooz, L., Smoot, J., & Abbaspourrad, A. (2024). Food LEGO: Building hollow cage and sheet superstructures from starch. *Science Advances, 10*(7), Article eadi7069. https://doi.org/10.1126/sciadv.adi7069

Koganti, N., Mitchell, J. R., Ibbett, R. N., & Foster, T. J. (2011). Solvent effects on starch dissolution and gelatinization. *Biomacromolecules, 12*(8), 2888–2893. https://doi.org/10.1021/bm200390a

Lauke, B. (2008). On the effect of particle size on fracture toughness of polymer composites. *Composites Science and Technology, 68*(15), 3365–3372. https://doi.org/10.1016/j.compscitech.2008.09.011

Li, P., Kierulf, A., Wang, J., Yaghoobi, M., Whaley, J., Smoot, J., … Abbaspourrad, A. (2022). Fabrication of charged self-assembling patchy particles templated with partially gelatinized starch. *ACS Applied Materials & Interfaces, 14*(21), 24955–24963. https://doi.org/10.1021/acsami.2c04738

Li, P., Li, J., Levin, J., Kierulf, A., Smoot, J., Zarei, A., & Abbaspourrad, A. (2024). Crafting tunable hollow particles using antisolvent-driven interlocking of micron-sized building blocks. *Advanced Functional Materials*, 2313025. https://doi.org/10.1002/adfm.202313025. n/a(n/a).

Li, P., McClements, D. J., & Decker, E. A. (2020). Application of flow cytometry as novel technology in studying the effect of droplet size on lipid oxidation in oil-in-water emulsions. *Journal of Agricultural and Food Chemistry, 68*(2), 567–573. https://doi.org/10.1021/acs.jafc.9b04956

Li, S., Moosa, B. A., Croissant, J. G., & Khashab, N. M. (2015). Electrostatic assembly/disassembly of nanoscaled colloidosomes for light-triggered cargo release. *Angewandte Chemie, 127*(23), 6908–6912. https://doi.org/10.1002/ange.201501615

Liu, X., Lan, C., Al, A., Yu, L., & Zhou, S. (2016). Preparation of cross-linked high amylose corn-starch and its effects on self-reinforced starch films. *International Journal of Food Engineering, 12*(7), 673–680. https://doi.org/10.1515/ijfe-2015-0139

Majzoobi, M., & Farahnaky, A. (2021). Granular cold-water swelling starch; properties, preparation and applications, a review. *Food Hydrocolloids, 111*, Article 106393.

Mewis, J., & Wagner, N. J. (2012). *Colloidal suspension rheology*. Cambridge university press.

Mezzenga, R., Schurtenberger, P., Burbidge, A., & Michel, M. (2005). Understanding foods as soft materials. *Nature Materials, 4(10), Article 10*. https://doi.org/10.1038/nmat1496

Narayanan, D., Nair, S., & Menon, D. (2015). A systematic evaluation of hydroxyethyl starch as a potential nanocarrier for parenteral drug delivery. *International Journal of Biological Macromolecules, 74*, 575–584. https://doi.org/10.1016/j.ijbiomac.2014.12.012

Punia Bangar, S., Sunooj, K. V., Navaf, M., Phimolsiripol, Y., & Whiteside, W. S. (2024). Recent advancements in cross-linked starches for food applications- a review. *International Journal of Food Properties, 27*(1), 411–430. https://doi.org/10.1080/10942912.2024.2318427

Samanta, B., Patra, D., Subramani, C., Ofir, Y., Yesilbag, G., Sanyal, A., & Rotello, V. M. (2009). Stable Magnetic Colloidosomes via Click-Mediated Crosslinking of Nanoparticles at Water–Oil Interfaces. *Small, 5*(6), 685–688. https://doi.org/10.1002/smll.200801659

Shintake, J., Cacucciolo, V., Floreano, D., & Shea, H. (2018). Soft robotic grippers. *Advanced Materials, 30*(29), 1707035. https://doi.org/10.1002/adma.201707035

Silverstein, R., Webster, F., Kiemle, D., & Bryce, D. (2014). *Spectrometric identification of organic compounds* (Eight ed.). NJ: John Willey & Sons. Inc.

Sjöö, M., Emek, S. C., Hall, T., Rayner, M., & Wahlgren, M. (2015). Barrier properties of heat treated starch Pickering emulsions. *Journal of Colloid and Interface Science, 450*, 182–188. https://doi.org/10.1016/j.jcis.2015.03.004

Tanner, R. I. (2018). Aspects of non-colloidal suspension rheology. *Physics of Fluids, 30* (10), Article 101301.

Walsh, A., Thompson, K. L., Armes, S. P., & York, D. W. (2010). Polyamine-functional sterically stabilized latexes for covalently cross-linkable colloidosomes. *Langmuir, 26* (23), 18039–18048. https://doi.org/10.1021/la103804y

Wu, M., Li, Y., Li, J., Xu, S., Gu, Z., Cheng, L., & Hong, Y. (2022). Preparation and structural properties of starch phosphate modified by alkaline phosphatase. *Carbohydrate Polymers, 276*, Article 118803. https://doi.org/10.1016/j.carbpol.2021.118803

Zhang, T., Hong, S., Zhang, J.-R., Liu, P.-H., Li, S., Wen, Z., … Corke, H. (2024). The effect of lactic acid bacteria fermentation on physicochemical properties of starch from fermented proso millet flour. *Food Chemistry, 437*, Article 137764. https://doi.org/10.1016/j.foodchem.2023.137764

Zhu, F. (2019). Starch based Pickering emulsions: Fabrication, properties, and applications. *Trends in Food Science & Technology, 85*, 129–137. https://doi.org/10.1016/j.tifs.2019.01.012